

The needle in the haystack - Where to look for more isolated cooling neutron stars

B. Posselt^{1,2,3}, S.B. Popov⁴, F. Haberl¹, J. Trümper¹, R. Turolla⁵, R. Neuhäuser², and P.A. Boldin⁶

¹ Max-Planck-Institut für extraterrestrische Physik, Postfach 1312 85741 Garching, Germany

² Astrophysikalisches Institut und Universitäts-Sternwarte, Schillergäßchen 2-3, 07745 Jena, Germany

³ Observatoire Astronomique de Strasbourg, 11 rue de l' Université, 67000 Strasbourg, France
e-mail: bposselt@cfa.harvard.edu

⁴ Sternberg Astronomical Institute, Universitetski pr. 13, 119991 Moscow, Russia
e-mail: polar@sai.msu.ru

⁵ University of Padua, Department of Physics, via Marzolo 8, 35131 Padova, Italy

⁶ Moscow Engineering Physics Institute (State University), Moscow, Russia

ABSTRACT

Context. Isolated cooling neutron stars with thermal X-ray emission remain rarely detected objects despite many searches investigating the ROSAT data.

Aims. We simulate the population of close-by young cooling neutron stars to explain the current observational results. Given the inhomogeneity of the neutron star distribution on the sky it is particularly interesting to identify promising sky regions with respect to on-going and future searches.

Methods. Applying a population synthesis model the inhomogeneity of the progenitor distribution and the inhomogeneity of the X-ray absorbing interstellar medium are considered for the first time. The total number of observable neutron stars is derived with respect to ROSAT count rates. In addition, we present sky maps of neutron star locations and discuss age and distance distributions of the simulated neutron stars. Implications for future searches are discussed.

Results. With our advanced model we can successfully explain the observed $\log N - \log S$ distribution of close-by neutron stars. Cooling neutron stars will be most abundant in the directions of rich OB associations. New candidates are expected to be identified behind the Gould Belt, in particular in the Cygnus-Cepheus region. They are expected to be on average younger and then hotter than the known population of isolated cooling neutron stars. In addition, we propose to use data on runaway stars to search for more radio-quiet cooling neutron stars.

Key words. stars: evolution — stars: neutron — X-rays: stars

1. Correction remark – added March 2010

Working on the new version of our population synthesis code, we recently discovered a bug in the version used in Posselt et al. (2008). This bug concerns the application of the improved ISM models to calculate the absorbed X-ray flux. The code erroneously did not cover the whole Galactic coordinate (l, b) range of the ISM-models to obtain the absorbing column density $N(H)$. Instead, only a small region ($\Delta l \approx 7$ deg, $\Delta b \approx 7$ deg) around the Galactic Center was used, which led to a significant overestimation of the absorption translating into an underestimation of the predicted neutron star number.

While all our main conclusions remain valid we add notes on some details regarding the corrected results in the Appendix A. Updated figures are shown in the Appendix A as well. It is mentioned in boldface in the text when there is an updated result available.

We note that this is the only paper, where the presented results are influenced by the bug in our population synthesis code. Previous works do not use it, and subsequent works like, e.g., Popov et al. (2010) have already applied the corrected version of the population synthesis code.

2. Introduction

More than 10 years after the discovery of its brightest member RX J1856-3754 (Walter et al. 1996), the small group of seven radio-quiet isolated neutron stars (NSs) detected by the ROSAT satellite have gained an important place in the rich zoo of compact objects. Together with Geminga and several close-by young radio pulsars, these objects form the local population of cooling NSs. Studies of this group of sources already provided a wealth of information on NSs physics (see e.g. Haberl 2007; Page et al. 2007; Zane 2007 for recent reviews).

Since 2001 the number of known close-by radio-quiet NSs has not been growing despite all attempts to identify (mainly in the ROSAT data) new candidates. Partly this is due to the fact that all these searches are blind, i.e. not necessarily targeted to promising sky regions. To advance the identification of new near-by cooling NSs it is necessary to perform a realistic modeling of this population. The seven ROSAT radio-quiet NSs form the main part of the known local population of cooling NSs. For these seven sources we use the term *Magnificent Seven*. There is still no general term to address the whole population to which these sources belong (terms such as XDINS – X-ray dim isolated NSs, DINS – dim isolated NSs, RINS – ROSAT (or ra-

radio quiet) isolated NSs, are used sometimes by different authors). In this paper we use the term ICoNSs (Isolated Cooling NSs). In our opinion, this variant better reflects the nature of these sources than, for example, XDINS, as many of them are not dim in X-rays. Finally, we call *coolers* all NSs, whose residual thermal emission can be detected. Besides the radio-quiet NSs, such sources can be also known as normal radio pulsars, or they may demonstrate some kind of radio emission or even γ -ray emission distinct from classical pulsars. In this study we do not care if an object shows some activity in addition to thermal surface emission. The only crucial point is the detection of X-ray emission related to the cooling of initially hot compact objects.

The population synthesis (PS) approach is used here to investigate the population of close-by young cooling NSs. There are two main versions of this method (Fritze-v. Alvensleben 2000). One, which sometimes is also called *empirical population synthesis*, is a kind of top-down approach, when objects, for which only integral characteristics are available, are studied. Numerical models are applied to reproduce observed properties of such sources by using different sets of subpopulations which constitute an object class. For example, the stellar content of a galaxy can be derived by modeling its integral spectra.

Here, we focus on the second – bottom-up – approach, often called *evolutionary synthesis*. In this case the evolution of a population of objects is modelled from their birth based on defined initial distributions of parameters and some equations which describe evolution of these distributions in time. The main reasons to use this second technique are the following. At first, if initial parameters or/and evolutionary laws for some kind of sources are not well known, then this kind of PS can be applied to test hypotheses about these uncertain properties by comparison between modeled and observed populations. Determination of the initial parameters of radio pulsars can be a good example here (Faucher-Giguère & Kaspi 2006). Next, even if the initial distributions and their evolution are known, but at the moment just a small part of the population – a tip of an iceberg – is observed, then PS calculations can be used to predict properties of the unobserved faint part of the population, and to plan a search strategy to identify new members. A more detailed review of the PS technique can be found, for example, in Popov & Prokhorov (2004).

In this paper an upgraded population synthesis model is discussed for the population of close-by (< 3 kpc) isolated NSs which can be observed via their thermal emission in soft X-rays. Previously, our models were applied to confirm the link between the Magnificent Seven and the Gould Belt (Popov et al. 2003) and to test theories of thermal evolution of NSs (Popov et al. 2006). The major interest of the present study is to understand how to find more objects of this type. After the description of the PS model ingredients in Sec. 3, we present our results – $\log N$ - $\log S$ -curves, age and distance diagrams as well as sky maps of expected NS locations – in Sec. 4, and discuss possible applications in Sec. 4.4. An outlook concerning the search for ICoNSs is given in Sec. 4.5 Finally, we give our conclusions in Sec. 5.

3. The new population synthesis model

The main physical ingredients which constitute our population synthesis model are the following:

- (A) the initial NS spatial distribution and the NS birth rate;
- (B) the kick velocity distribution of the NSs;
- (C) the Galactic gravitational potential;
- (D) the distribution of NS masses, in the following: NS mass spectrum;
- (E) the NS cooling curve;
- (F) the NS surface emission in X-rays;
- (G) the interstellar absorption of X-rays;
- (H) the properties of the X-ray detector.

At each time step in the simulation we consider at the same time eight different NS masses with corresponding cooling curves, following each NS on its trajectory through space and time until it is too faint to be observed. The overall result of, e.g. 50000×8 simulated NS evolutionary tracks from birth till the time when the temperatures falls below 10^5 K, is normalised by the mass distribution as well as by birth rates (see below for both). Ingredients B, C, E, and F are unchanged with respect to our previous studies (Popov et al. 2003, 2005, 2006, hereafter Paper I, II, III), so we just briefly comment on them below. The ingredients A, D, G, and H – the initial spatial distribution, the NS mass spectrum, the interstellar absorption, and the X-ray detector properties – are modified, and they are described in subsections below in more details.

For the kick velocity distribution (B) of newborn neutron stars we use that proposed by Arzoumanian et al. (2002), as in all our previous studies. This is a bimodal distribution, consisting of two Maxwellians with most probable velocities $V_{\text{peak1}} \approx 127$ km s $^{-1}$ and $V_{\text{peak2}} \approx 707$ km s $^{-1}$, the average velocity is ≈ 527 km s $^{-1}$. Recently, this assumption was criticized. A single-component distribution with $V_{\text{peak}} \approx 400$ km s $^{-1}$ was advocated by Hobbs et al. (2005), and by Faucher-Giguère & Kaspi (2006) who accepted a non-Maxwellian velocity distribution. However, since all objects under study are very young and so still are relatively close to their birth place, the exact shape of the velocity distribution does not have a strong influence on our final results.

The calculation of NS trajectories in the Galactic gravitational potential (C) follows that presented in Papers I and II. As before we use the axisymmetric Miyamoto-Nagai (1975) potential with disc, buldge and halo contributions. This potential (with some modifications) was actively used in NS calculations by different authors already in the 1990s (see, for example, Blaes & Madau (1993) and references therein). Again, it is noted that since the NS are young the use of a very precise multicomponent potential is not necessary. Thus, we neglect also the Galactic bar which extends to a maximum Galactocentric distance of 3.5 kpc (e.g. Pichardo et al. 2004) because its influence is very small for the relatively nearby objects of interest.

The thermal evolution of NSs is one of the main ingredients of the study. There are strong uncertainties in this topic. Sets of curves have been calculated by many research groups for different models of NS interiors (see a reviews, e.g. by Page & Reddy 2006 or Yakovlev & Pethick 2004). In the following we consider only hadron stars and use cooling curves (E) corresponding to those marked as model I in Paper III. This cooling model includes the following important ingredients. Superfluid gaps are taken according to Takatsuka & Tamagaki (2004). Medium modifications of the neutrino processes are taken into account. Formation of the pion condensate is possible. The relation between tem-

peratures of the outermost core layer and the surface is taken from Blaschke et al. (2004). No additional heating is used.

In our calculations we do not account for atmospheric reprocessing of the thermal radiation, and assume that the emitted spectrum is a pure blackbody (see a detailed description of the modeling of the observed neutron star thermal emission in Zavlin 2007). Unfortunately, the distribution of the chemical compositions of atmospheres is not known for the whole population of young NSs. If the atmospheric composition changes in time or not is also unclear. As an additional parameter one needs further to consider the (unknown) magnetic field strength and its effects on the atmosphere. So, the available data are not complete enough and statistics is too low to consider atmospheres in population synthesis studies.

However, isotropic blackbody emission is a simplification since there is growing evidence that the thermal X-ray emission observed in case of the Magnificent Seven actually comes from hot spots and not from the whole NS surface (e.g. Haberl et al. 2006; Schwöpe et al. 2005; Trümper et al. 2004). This is expected to influence not only the cooling times but also the detection probabilities. But the overall quantitative effect is currently unclear as at first it is necessary to include non-uniform heat transport in the outer NS layers into cooling curves calculations self-consistently, for example, in the way it is discussed in Aguilera et al. (2007a). Strong toroidal magnetic fields produce hot spots and can keep them hot over a longer time than the usual lifetime expected from the previous cooling models (Page et al. 2007).

Since the hot spot of a neutron star will have a higher temperature than in the case of isotropic cooling, its detection would be less affected by interstellar absorption. The fact that these effects are not accounted for by our applied cooling curves leads to underestimating the number of observable neutron stars. On the other hand, Yakovlev & Pethick (2004) have pointed out that at high magnetic field strength the break of the cooling curves (marking the transition from neutrino to photon cooling) shifts towards lower ages, viz. from $\sim 10^6$ years at $B \sim 0$ G to a few times 10^5 years for magnetic fields typical for the Magnificent Seven, $B \sim 10^{13} - 10^{14}$ G. Neglecting this effect will lead to an overestimate of the number of observable neutron stars with ages of $(0.5-1) \times 10^6$ years where some of the Magnificent Seven are found. Magnetic field decay and the additional heating due to it (Aguilera et al. 2007b) can further increase the number of observable NSs. We cannot make a firm prediction about the net change to the $\log N - \log S$ which is caused by these effects which are partly counterbalancing. However, we believe that the blackbody estimate of the count rate S is reliable within a factor of ~ 2 .

The soft X-ray spectra of objects under consideration are well fitted by the blackbody shape, and, more important, the cooling curves used here were calculated under the assumption of blackbody emission of the whole NS surface, and cooling curves for non-uniform emission are currently not publicly available. We therefore stick to the cooling curves of paper III and the assumption of spherical symmetric blackbody emission, and apply them as a reference model to study the main aspect of this paper - the influence of the inhomogeneous distributions of neutron star birth places and interstellar absorptions in the Galaxy.

3.1. Initial spatial distribution of NSs

Following the results of previous investigations (paper I), we take as established that the population of nearby NSs is genetically related to the Gould Belt. The contribution of the Gould Belt dominated the production of compact remnants in the solar proximity over the past ~ 30 Myrs (see Pöppel 1997 for a detailed description of the Gould Belt structure). About two thirds of massive stars in the ~ 600 pc around the Sun belong to the Gould Belt (Torra et al. 2000).

In paper I and II we considered that NSs are born either in the Belt or in the Galactic disc, both treated as infinitesimally thin, disc-like structures, with a uniform spatial distribution. The total NS birth rate in the Galactic disc (the whole area inside 3 kpc) and that in the Gould Belt alone were taken to be 270 Myr^{-1} and 20 Myr^{-1} , respectively. The first value corresponds to the value inside 1 kpc by Tammann et al. (1994). The latter value is from Grenier (2000), and appears in reasonable agreement with the historical supernova rate inside 1 kpc, as estimated by Tammann et al. (1994).

Here, the previously simplified progenitor distribution is significantly upgraded by adopting a more realistic description of the massive star geography in the solar neighborhood. In particular, in the innermost 500 pc from the Sun the initial spatial distribution of NSs is assumed to follow the presently observed distribution of massive stars. Outside the well-known 500 pc and up to 3 kpc, NSs are born either in the Galactic disc, assumed to be exponential both in z and R directions, or originate from known, rich OB associations.

3.1.1. Inside 500 pc

For the stars inside 500 pc we use the *Hipparcos* data on massive stars (Perryman & ESA 1997). Our assumption is that the present day distribution of massive stars represents their distribution in the last 1-2 million years well.

All the 570 classified B2-O8 stars with known parallaxes $> 0''.002$ are considered. According to the birthrates above in our model 27 (out of 270) NS producing supernova events per Myr are assumed to be related to this population. This number should be compared with 20 NSs assumed to be born in the entire Gould Belt in 1 Myr in our old model. The parameters of the new model roughly lie in between the old one for $R_{\text{Belt}} = 300$ and 500 pc.

In the code the initial position of each newborn NS coming out of this population coincides with the position of one of these 570 *Hipparcos* stars. This assumes that the spatial distribution of the massive main sequence stars does not change significantly over the NS evolutionary timescale (≈ 1 Myr). A progenitor star is chosen randomly, but we tried to account for the probability for each particular star to explode. Since for each star the spectral type is known, one can roughly estimate its mass. The mass interval corresponding to each spectral type gives us an estimated range for its total lifetime. If one has no information about the age of the star then the probability is assumed to depend just on the star's full lifetime: the probability is higher for more massive stars as they are shorter lived (actually, the probability to explode is inversely proportional to the lifetime of the star).

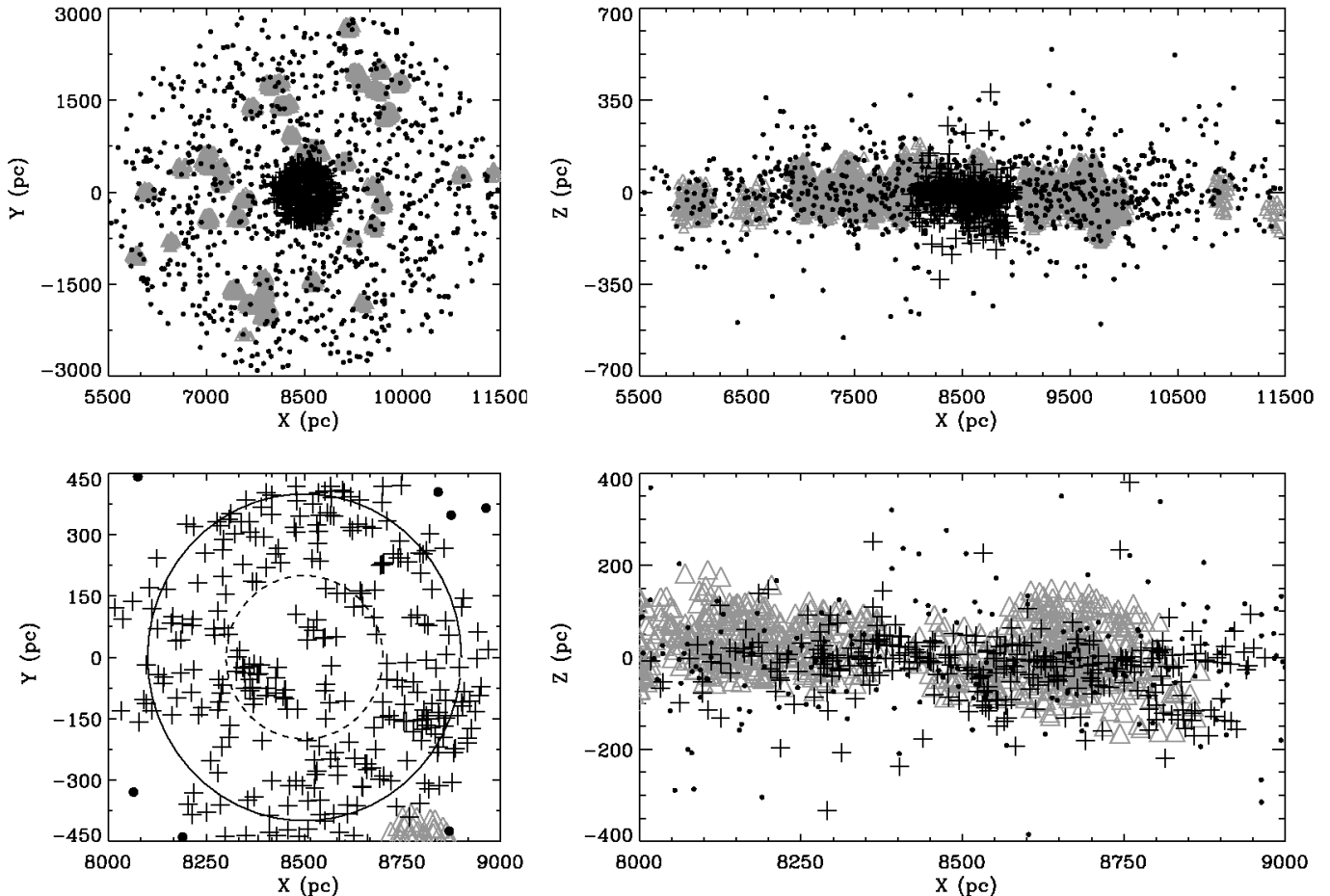


Fig. 1. The new NS progenitor distribution. The grey triangles represent the stars in the OB associations. Crosses stand for the considered *Hipparcos* stars inside 500 pc. Small circles mark random stars in the Galactic disc ($500 < d < 3000$ pc). Outside 500 pc from the Sun two populations are visible: NSs formed in OB associations, and NSs formed in the field. Bottom panels show the projected distribution X-zoomed to 500 pc around the Sun. Two circles on the bottom left panel are plotted with radii of 200 and 400 pc from the Sun.

As noted above, the mass interval corresponding to each spectral class is converted into an approximate limiting lifetime: T_{LM} is the longest lifetime for the lowest mass, and T_{HM} is the shortest lifetime for the high mass end of the particular mass interval. If the star is known to belong to an OB association, we also consider the age of the OB association. The ages of the OB associations are shown in Table 1; they are taken from de Zeeuw et al. (1999). In several cases de Zeeuw et al. (1999) give just one number (not a range) as an estimate of an age. Of course, these numbers have some uncertainty. To account for this we added an uncertainty (± 1 Myr) in all those cases. By this we have for all OB associations in the Table T_{LOB} and T_{UOB} , a lower and upper age limit for the OB association, respectively.

The probability for a progenitor star to explode (and so to contribute to NS production in our model) is estimated as follows.

(i) If $T_{HM} > T_{UOB}$, then the probability of a star exploding is zero, as the shortest estimated lifetime is longer than the age of the OB association. Such stars do not contribute to NS production in our model, i.e. no compact objects could have been born at their locations because the OB association is too young.

- (ii) Conversely, if $T_{LM} < T_{LOB}$ then the probability is inversely proportional to the longest lifetime, T_{LM} , of the star. This probability is also used for stars not belonging to OB associations within a 500 pc distance.
- (iii) If $T_{HM} < T_{LOB}$ but $T_{LM} > T_{UOB}$ then the probability is inversely proportional to $(T_{UOB} - T_{LOB})$, as one has to consider overlapping time scales.
- (iv) If $T_{HM} < T_{LOB}$ and $T_{LOB} < T_{LM} < T_{UOB}$ then the probability of exploding is inversely proportional to $(T_{LM} - T_{LOB})$.
- (v) If $T_{LOB} < T_{HM} < T_{UOB}$ and $T_{LM} > T_{UOB}$ then the probability is inversely proportional to $(T_{UOB} - T_{HM})$.
- (vi) If $T_{LOB} < T_{HM}$, but $T_{LM} < T_{UOB}$ then the probability of exploding is inversely proportional to the minimum time value $(T_{LM} - T_{HM})_{MIN} = 1.44$ Myr, which was obtained for the spectral type B0 corresponding to the mass interval $[15 M_{\odot}, 18 M_{\odot}]$.

To summarize, the initial spatial distribution of NSs inside 500 pc in our model follows the distribution of *Hipparcos* massive stars weighted by their explosion probabilities as estimated above. Outside 500 pc this weighting is not applied.

3.1.2. Outside 500 pc, up to 3 kpc

Most of the NSs in our model, 200 out of 270 per Myr, are born in one of 49 OB associations outside 500 pc and up to 3 kpc. The radii of the association extents are taken to be equal to 100 pc. This is a safe upper limit on their sizes, as usually diameters are about 80 pc, and up to 200 pc (Mel'nik & Efremov 1995). The probability to be born inside this radius is uniform. We assume that the number of stars with known photometry roughly reflects the total number of stars in the cluster. The probability to be born in each cluster is proportional to this quantity. The data on the 49 OB associations are taken from the catalogue by Blaha & Humphreys (1989) (see also Mel'nik & Efremov 1995). Note, that distances to the associations are reduced by 20% according to conclusions by Dambis et al. (2001).

Finally, out of the total 270 NSs, 43 are supposed to be born during 1 Myr in the Galactic disc outside 500 pc from the Sun, but inside 3 kpc. Their positions in the disc are calculated randomly. The disc is exponential both in R and Z . For the disc Z -scale we take the value 100 pc. For the radial scale we take the value 3 kpc (Kent et al. 1991; Fux & Martinet 1994).

In our model the NS formation rate outside 500 pc around the Sun corresponds to $\sim 0.884 \cdot 10^{-11} \text{ pc}^{-2} \text{ yr}^{-1}$. This rate is lower than the one stated by Tammann et al. (1994). They, adopting that the Milky Way is type Sbc, and combining the corresponding value with the historical rate in the Galaxy, reported a local SN rate of $2 \cdot 10^{-11} \text{ pc}^{-2} \text{ yr}^{-1}$. Tammann et al. (1994) gave also a rate of $2.9 \cdot 10^{-11} \text{ pc}^{-2} \text{ yr}^{-1}$ which is based on the census of O-B2 stars in 1 kpc around the Sun. Clearly, both values should be dominated by the productive Gould Belt. Outside the Belt the rate should be lower, however, it should be anisotropic and non-uniform on the scale of 3 kpc. Our adopted values, $\sim 3.438 \cdot 10^{-11} \text{ pc}^{-2} \text{ yr}^{-1}$ inside 500 pc and $\sim 0.884 \cdot 10^{-11} \text{ pc}^{-2} \text{ yr}^{-1}$ outside 500 pc are chosen to reflect this fact. At the 500 pc transition our model gives comparable values due to the scaling through OB associations. We checked that at this transition our model distance distribution of *unabsorbed* NS show consistently increasing numbers. Probably, we slightly underestimate the NS formation rate at larger distances in the directions of the Galactic center and spiral arms. However, for our calculations closer regions are more important (see distance distributions of

ICoNSs below). Anyway, we warn the reader that some uncertainty in the birth rate normalization is hidden inside our model. Comparison of the Log N – Log S distribution for old and new models of the initial spatial distribution of NSs is made in Fig. 3 and discussed in Sec. 4.

3.2. The interstellar absorption of X-rays

X-rays are absorbed by the heavy elements of the interstellar medium. This is especially true for the soft X-rays below 1 keV. Their extinction has to be accounted for if one aims at realistic estimates of the sources observability. The amount of material between the object and the observer is measured as hydrogen column density $N(H)$. Then, assuming the same abundances towards all directions and accounting for photoelectric absorption processes by atoms, ions and dust particles one can determine the X-ray extinction. The treatment of X-ray absorption is significantly upgraded in our new population synthesis with respect to previous studies by considering all these aspects, i.e. a more realistic model for $N(H)$, up-to-date abundance tables and cross sections (see Posselt et al. (2007) for a more thorough discussion and paper III for details about previous treatment of the ISM absorption¹).

In the following we use the abundance tables and photoelectric cross sections by Wilms et al. (2000) as combined in the `tbabs` routine which is implemented e.g. in XSPEC². We also introduce two different, new $N(H)$ models in three dimensions to account for the highly inhomogeneous distribution of the interstellar medium (ISM). Both models take into account the most updated results in the local neighborhood (up to 230 pc) by Lallement et al. (2003). Their work well describes the local bubble which is surrounded by clumps of denser ISM and connected by chimneys to other bubbles. For distances larger than 230 pc we use the analytical ISM model described in Popov et al. (2000) in one of our new $N(H)$ models, in the following it is named “analytical ISM model”. For the second $N(H)$ model we use the extinction study by Hakkila et al. (1997). In the following we refer to this model as the “Hakkila ISM model”.

Concerning the transition region at 230 pc we want to make the following short comments. The column density can only increase with larger distance, thus the new data from the analytical formulae / the Hakkila study are only applied if the resulting column densities are larger than those from Lallement et al. (2003) at 230 pc. At distances larger than 230 pc the models become naturally much coarser due to fewer measurements. For the analytical model the transition is smooth since the analytical formulae at, e.g., 240 pc result in values similar to the ones at 230 pc by Lallement et al. (2003). In case of the Hakkila model the transition is more abrupt due to the patchiness of the available measurement data applied for the extinction study by Hakkila et al. (1997). On *average* the hydrogen column density at around 230 pc is around 10^{20} cm^{-2} . This *average* value increases by around 10^{20} cm^{-2} at the transition for

OB association	Age [Myrs]
Upper Scorpius	4-6
Upper Centaurus Lupus	12-14
Lower Centaurus Crux	9-11
Vel OB2	6-10
Trumpler 10	15-30
Collinder 121	4-6
Ori OB1	9.5-13.3
Per OB2	3-7
α Persei (Per OB3)	25-50
Cas-Tau	25-50
Lac OB1	2-25
Cep OB2	5-10
Cep OB6	25-50

Table 1. OB associations inside 500 pc and their ages (from de Zeeuw et al. 1999). For Ori OB1 the age proposed for its older part Ori OB1A is taken.

¹ We also corrected in the old ISM model the use of full widths of half maximum instead of the required variances in the exponential density factors by Zane et al. (1995); Dickey & Lockman (1990). However, the effect of smaller ISM density above the Galactic plane on our model results was quite low.

² <http://heasarc.gsfc.nasa.gov/docs/xanadu/xspec/>

the Hakkila model, while in case of the analytical model the *average* increase is only around 10^{19} cm^{-2} .

Both models were checked with open cluster extinction data which were presented by Kharchenko et al. (2005a,b) and Piskunov et al. (2006) and are complete up to a distance of 850 pc. The data of the open clusters were then included in both models (see Posselt et al. (2007) for details on the models). The column densities derived from both ISM models at large distances were also compared with the results by Schlegel et al. (1998) from infrared dust emission measurements. In both cases, the analytical ISM model and the Hakkila ISM model, data cubes in Galactic coordinates (steps of one degree) and distance (steps of 10 pc) are used for our population synthesis. The sampling of the data cube does not reflect the actual accuracy, which is around 25 pc within 230 pc and much coarser at larger distances.

It is noted that the both models are large-scale models and even the Hakkila ISM model does not account for small ISM clumps, especially at large distances, above 1 kpc.

3.3. Mass spectrum

NS cooling curves strongly depend on masses. Once the cooling scenario is chosen, it is therefore necessary to specify the NS's mass spectrum. As in our previous studies, we use the mass spectrum of NS which is derived by the joint use of *Hipparcos* data on spectral classes of close-by massive stars and calculations by Woosley et al. (2002). In addition, in this paper a modified mass spectrum is studied obtained by using the calculations from Heger et al. (2005).

Both mass spectra are obtained in a similar way, and *a priori* it is impossible to say that the “new” one is preferable with respect to the “old” one. We take spectral types of massive stars around the Sun as given in the *Hipparcos* catalogue (Perryman & ESA 1997). To each spectral type we associate a range of masses. Applying now the calculations by Woosley et al. (2002) or, instead, by Heger et al. (2005) we obtain the baryonic masses of compact objects. Then the baryonic masses are translated into gravitational masses by using the simple equation, valid for hadronic NSs, by (Timmes et al. 1996)

$$M_{\text{bar}} - M_{\text{grav}} = 0.075 M_{\text{grav}}^2.$$

The accuracy of this relation is sufficient for our purposes, as one needs to know the mass within a few percent (less than half the size of a mass bin). Finally, we have a mass spectrum with eight mass bins which correspond to the eight cooling curves we use in our calculations.

In Fig. 2 the used two mass spectra are shown – the old (dotted line in the graph) mass spectrum which we also used in previous studies, and the new one. Note the non-equal widths of the mass bins. Eight cooling curves for gravitational masses 1.1, 1.25, 1.32, 1.4, 1.48, 1.6, 1.7, and $1.76 M_{\odot}$ are taken, both in the new and old mass spectrum. Each bin boundary corresponds to the mean between two values of mass used in calculations.

For the old spectrum in Fig. 2 we use the relation between a progenitor mass and NS baryonic mass derived from Fig. 17 by Woosley et al. (2002). We approximate the data in this figure with two linear relations (for progenitor masses $< 15 M_{\odot}$ and $> 25 M_{\odot}$, respectively), and constant between 15 and 25 solar masses (see Paper II). A peak at $1.4 M_{\odot}$ appears due to the fact that in this region pro-

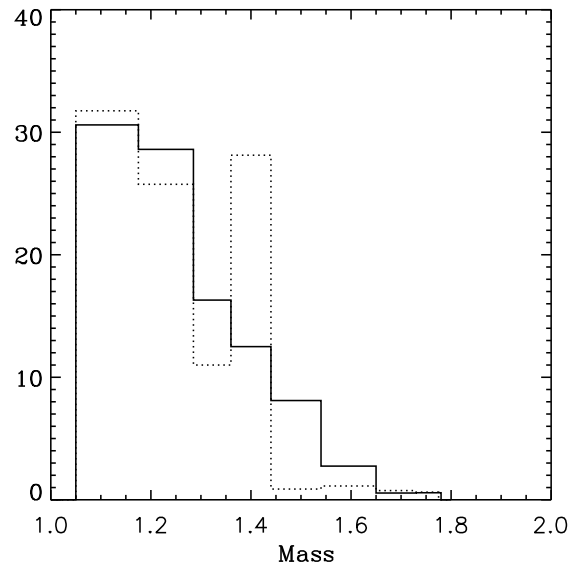


Fig. 2. The old (as used in previous studies, dotted line) and the new (as introduced in this work) mass spectra, binned over eight intervals of different widths (see the text).

genitors of different mass produce NSs of similar masses. The new mass spectrum, shown with a solid line, is derived much in the same way, but using data from Heger et al. (2005) for stars with masses $> 12 M_{\odot}$. As it is visible in the figure, the peak at $1.4 M_{\odot}$ disappears. This is because the dependence of the compact star mass on the progenitor mass contains no flat regions. The most important feature of both mass spectra is a very small number of NSs with masses above $\sim 1.5 M_{\odot}$. As the cooling of a NS is faster for massive stars, a small number of massive objects implies a small number of cold stars in the same age group.

3.4. Detector properties

As before (e.g. in Paper I) we use the instrumental response of ROSAT to draw conclusions with respect to the ROSAT All Sky Survey (RASS). However, the energy range considered, e.g. in Paper I was 0.08 keV to 3 keV while the RASS data analysis was done for a slightly smaller energy range. To be in full agreement we changed the energy range now to 0.1 keV to 2 keV. The effective area of the instrument is discontinuous over energy due to sharp instrumental absorption edges in the energy band of interest. With respect to previous studies our sampling of the effective area measurements was improved to better account for such absorption edges. In few cases we found differences of up to 40% in the resulting absorbed fluxes for an object. However, this effect is pronounced only for very soft sources at very small distances. Thus the influence on the overall results of the population synthesis are small. We note, that of course one has to consider vignetting of the X-rays as not all RASS sources are observed on-axis. This is done by an effective area measurement with averaged vignetting applicable for the RASS.

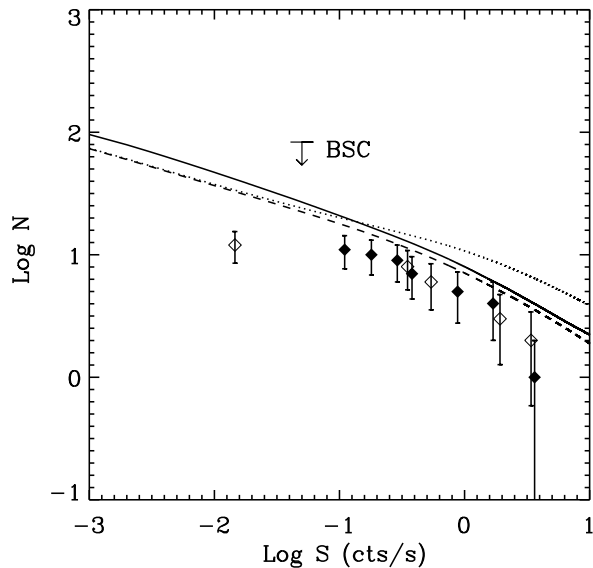


Fig. 3. Log N – Log S for the new initial spatial distribution (solid line) and two variants of the old spatial distribution with $R_{\text{belt}} = 300$ pc (dotted) and 500 pc (dashed). The curve shown as a solid line is used as reference on the following plots, too. This curve is calculated for the old mass spectrum, old ISM distribution, and new ISM element abundances. The data points represent the Log N - Log S distribution for the known young close-by isolated neutron stars with thermal X-ray emission (the Magnificent Seven, Geminga, the “second Geminga” – 3EG J1835+5918, and three radio pulsars: B0833-45, B0656+14, B1055-52). Filled symbols correspond to the Magnificent Seven, open symbols to the other NSs. Error bars are plotted for the poissonian errors. From the list in Popov et al. (2003) we removed PSR1929+10 since results of the recent XMM-Newton observations by Becker et al. (2006) demonstrate that the spectrum is non-thermal.

4. Results of calculations and discussion on the influence of model modifications

In this section we compare results of different modifications of the population synthesis scenario studied in this paper. We start by comparing the log N – log S distributions calculated with different assumptions, proceed to the resulting map of the cooling neutron star distribution on the sky, followed by age and distance distribution, and finally discuss the implications on searches for new ICoNS candidates.

4.1. Comparison of log N – log S distributions for different model modifications

The effects of the successive modifications in our PS-model on the log N – log S distribution are shown in Figs.3-5. The solid curve in all the figures is the same. It corresponds to the new initial spatial distribution of the NSs, new abundances and cross-sections, the old mass spectrum, and the old ISM model.

At first we discuss the influence of the new initial spatial distribution of NSs (i.e. distribution of progenitors). We compare three models: two variants of the old model with

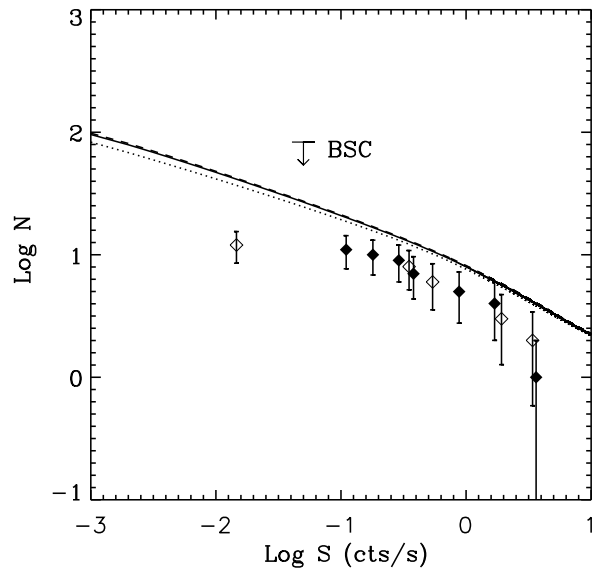


Fig. 4. In this figure we present the effect of the new mass spectrum and new ISM element abundances. All curves are plotted for the new initial spatial distribution of NSs. Solid curve: old mass spectrum and new abundances. Dotted line: old mass spectrum and old abundances. Dashed curve: new mass spectrum and new abundances. All curves are calculated for the old ISM distribution model.

$R_{\text{Belt}} = 300$ pc and 500 pc and the model with the new initial spatial distribution described in Sec. 3.1. Log N – Log S curves are shown in Fig. 3. Except for the initial spatial distribution all other parameters are the same: old mass spectrum (Fig. 2, dotted curve), new abundances, old ISM distribution (calculations with the new ISM distribution take long times, so for comparison of different modifications we use the old ISM distribution model when possible).

The solid curve corresponds to the new initial spatial distribution. The result with the new progenitor distribution lies in between those of the two old ones for large and moderate fluxes. In fact, our new calculation is only slightly above the simpler model with a Gould Belt radius of 500 pc. For count rates $\log S < -1$ the new initial spatial distribution results in roughly 0.1 dex more observable sources. The new model of the spatial distribution and the old for $R_{\text{Belt}} = 500$ pc are in reasonable correspondence with observations at the bright end, where it is supposed that our knowledge about observable objects is mostly complete (as we see below new models of the ISM distribution shift the curve down improving the correspondence). However, the locations of observable sources on the sky for the old and new initial spatial distributions are significantly different (compare Fig. 6 below and Fig. 6 in Paper II).

Next, one has to compare the Log N – Log S distributions calculated for different mass spectra (see Sec. 3.3). Computations were made for the new initial spatial NS distribution, new ISM element abundances and old ISM distribution. Results are shown in Fig. 4. To see the effect of the new mass spectrum one has to compare the solid and the dashed curves. The solid curve is the same as in Fig. 3. It corresponds to the old mass spectrum (Fig. 2, dotted line). The dashed curve, which is nearly indistinguishable

from the solid one, is calculated for the new mass spectrum (Fig. 2, solid line). Surprisingly, the two different mass spectra provide nearly the same result for the $\text{Log N} - \text{Log S}$. This is very positive for our approach since the mass spectrum is a poorly determined component of the model. As noted above, none of the mass spectra applied here is currently more preferable than the other. In the following we continue to use the “old” mass spectrum.

In Fig. 4 the effect of the new ISM element abundances is also shown. The dotted curve should be compared with the solid one. As it can be seen, the effect is not very important. Naturally, it more strongly influences faint sources, which are situated at larger distances (on average). However, even for far away sources the effect is not significant.

Finally, we compare the $\log N - \log S$ curves obtained for three different models of the ISM distribution. In Fig. 5 we show results for the old simple model (reference curve), the new analytical ISM model, and the Hakkila ISM model. The curve of the new analytical ISM model is very close to the one of the old ISM model for bright sources. As sources become fainter the number of observable objects becomes smaller than before due to the appearance of directions with high absorption. Using the Hakkila ISM model we obtain a $\log N - \log S$ curve which fits the known observational constraints even better. For small fluxes this curve approaches the reference one. In comparison to the analytical ISM cube there are large “windows” of low extinction in the Hakkila ISM model resulting in more sources at low fluxes. The analytical model on the other hand seems to overpredict the absorption when going to larger distances (Posselt et al. 2007). Thus, at fainter fluxes one may regard the results of the analytical and Hakkila ISM model as lower and upper limits on the number of observable sources.

We conclude, that in terms of the $\log N - \log S$ distribution our new, more realistic, models are in good agreement with the older ones. The interstellar absorption by the Hakkila ISM model results in a $\log N - \log S$ curve situated slightly closer to the known observations of INs.

By using a different set of cooling curves one may improve the agreement between computed and observed $\log N - \log S$ distributions. A detailed analysis is, however, outside the scope of the present investigation. Therefore, in the following only few comments are made regarding the set of cooling curves applied in our previous Paper III. As apparent from Fig. 3 and Fig. 5 our final $\log N - \log S$ curves which include the new ISM distribution models are not significantly different from the curve using $R_{\text{belt}} = 500$ pc in our old calculations (Paper III). So, the main conclusions about different sets of cooling curves presented in Paper III should not change. While the curve calculated in the case of the Hakkila ISM model – dashed in Fig. 5 – lies at low count rates slightly below the old curve with $R_{\text{belt}} = 500$, this deviation is not strong enough to validate the cooling models which have been rejected in Paper III. Moreover, for this choice of the ISM distribution the cooling models which have been considered as acceptable in Paper III fit even better the observations.

4.2. Sky maps

In earlier papers on population synthesis calculations we did not attempt to produce realistic sky maps of the ICoNS distribution, as some of our assumptions were quite crude.

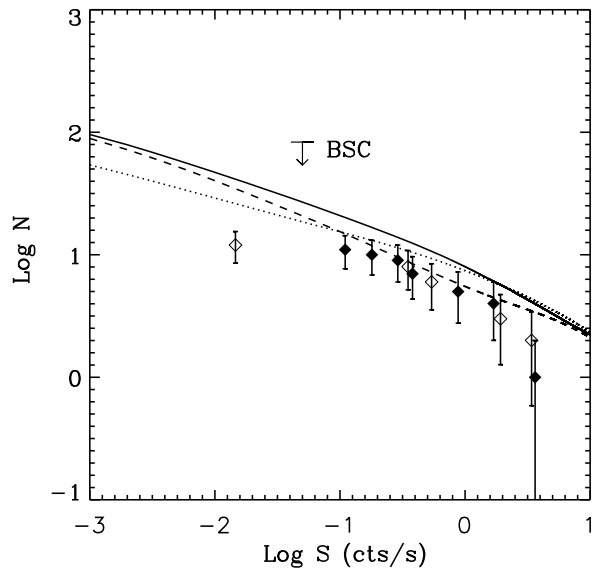


Fig. 5. $\text{Log N} - \text{Log S}$ in case of different X-ray absorbing ISM models. All curves are plotted for the new initial spatial distribution, the old mass spectrum and new ISM element abundances. Solid curve: old, simple analytical ISM model as e.g. in Paper III. Dotted curve: new improved analytical ISM model; dashed curve: Hakkila ISM model, see Sec. 3.2 **For an updated version of this figure see Fig. A.1 in the Appendix A.**

Now, with detailed distributions of ISM and birth places of NSs, one can try to compute such maps. In Fig. 6 we present a map in Galactic coordinates for the new initial spatial distribution of NSs, old mass spectrum and the new analytical ISM model. The plot shows the expected number density for sources with count rates > 0.05 cts s^{-1} . Obviously, sources appear to be restricted towards the Galactic plane and the plane of the Gould Belt. Few objects are expected to be found at latitudes higher than 30° (see, however, Sec. 4.5). Inside ± 30 degrees from the Galactic plane the distribution of sources is dominated by NSs from relatively close, rich OB associations. We mark by boxes the most important of them: Sco OB2, Cyg OB7, Cep OB3, and Ori OB1. Interplay between source distribution and 3D ISM structure allows us to make predictions on which directions are most promising for looking for new ICoNSs.

The computed distribution of sources in Fig. 6 is dominated by sources with count rates in the range $[0.05, 0.1]$ cts s^{-1} . This corresponds to the dimmest sources among identified radio and γ -ray silent ICoNS, or even to count rates smaller than < 0.1 cts s^{-1} where there aren't currently any ICoNS known. In the distribution of known ICoNSs (Motch et al. 2007) there are no sources with Galactic longitude in the range $\sim 50^\circ$ to $\sim 200^\circ$. At the first glance, this is in contradiction with our present map. However, it is necessary to note, that for brighter sources (> 0.5 cts s^{-1}) the Cygnus-Cepheus region does not give a strong contribution, and 1-2 objects could escape identification in this overcrowded area close to the Galactic plane (see Sec. 4.4 for a more detailed discussion).

In Fig. 7 we present a similar map for the same parameters concentrated on the faint sources having nominal

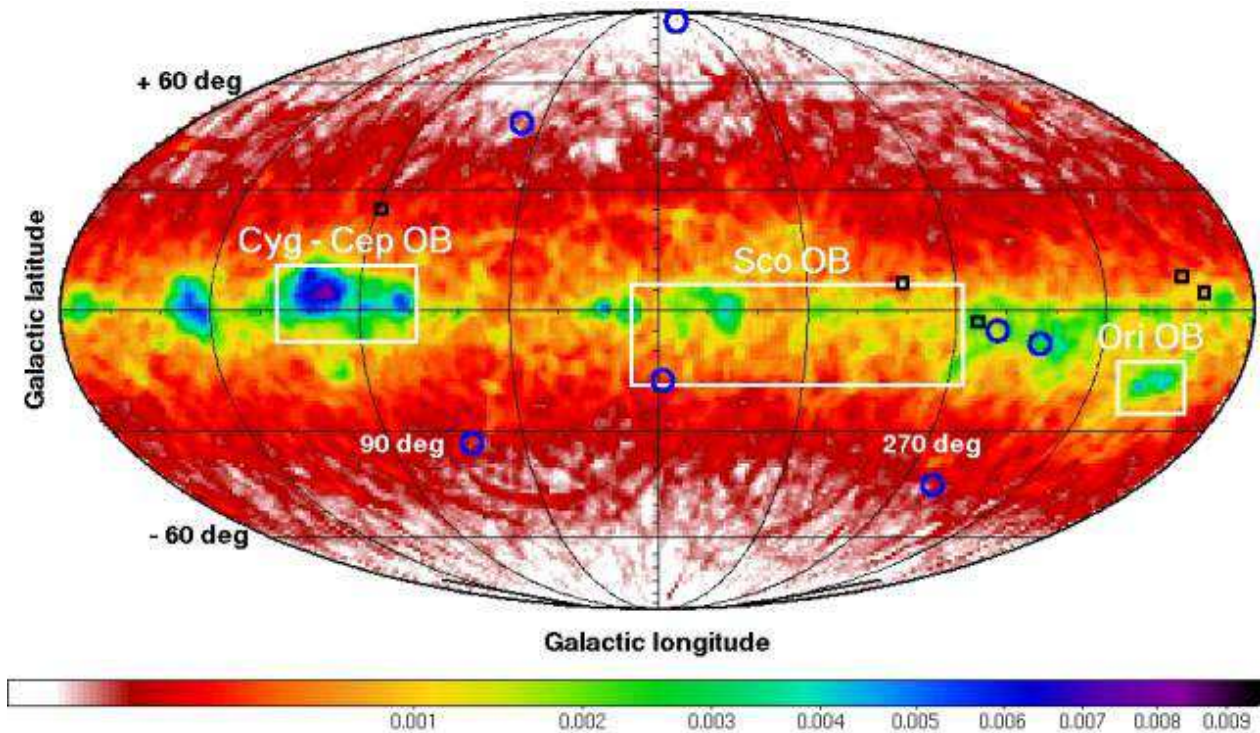


Fig. 6. The expected number density of isolated neutron stars with thermal X-ray emission in units of numbers per square degree. The Galactic map is in Mollweide projection. Only sources with ROSAT PSPC count rates larger than 0.05 cts s^{-1} are considered, the same value as used in Paper II in their Fig. 6. The simulation was done for new initial progenitor distribution, new abundances, old mass spectrum and the new analytical ISM model, thus corresponds to the dotted $\log N - \log S$ curve in Fig. 5. Marked in blue are the positions of the Magnificent Seven and in black the positions of close young radio pulsars with detected thermal X-ray emission. **For an updated version of this figure see Fig. A.2 in the Appendix A.**

ROSAT count rates between 0.001 cts s^{-1} and 0.01 cts s^{-1} . We note that the RASS is not so deep. Fig. 7 demonstrates the effect of more distant ($> 1 \text{ kpc}$) OB associations, the most important ones are marked in the map.

4.3. Age and distance distributions

In this paper we introduce age and distance distributions of close-by NSs as predicted by our PS model. These distributions can help to illustrate better the properties of both discovered and still elusive ICoNSs. Figures 8 and 9 show the computed age and distance distributions for NSs with ages up to 10^6 years with bin size 10^5 years, and distances up to 700 pc with bin size of 140 pc , calculated for different model assumptions (the two variants of the initial spatial distribution of NSs, and the three models of ISM distributions).

We start by presenting only the general picture and refer to Sect. 4.3.1 for a comparison of the impacts the different PS scenarios have on our results. Fig. 8 confirms the natural expectation that the youngest neutron stars contribute most to the observable object fraction in all flux ranges as they are both brighter and hotter. The radial distribution for different count rates is presented in Fig. 9. While for large fluxes most sources are situated in the region $\sim 200 - 400 \text{ pc}$ (ie. in the Gould Belt), for fainter objects the picture is different. At fluxes below $\sim 0.1 \text{ cts s}^{-1}$ one expects to see mostly sources behind the Gould Belt. These general features are very important, as they indicate that new, still

unidentified ICoNS are expected to be young objects behind the Gould Belt. We discuss this proposition below in Sec. 4.4.

4.3.1. Comparison of the distributions for the different model modifications

The population synthesis models used to obtain the results presented in Fig. 8 and Fig. 9 differ on the one hand in the initial progenitor distribution and on the other hand in the adapted ISM model. As it is already evident from the $\log N - \log S$ curve in Fig. 3 the predicted number of observable NSs is generally higher in the case of the new initial progenitor distribution compared (white bars) to the old one (vertically striped bars). The decrease in number from the youngest to the oldest sources for both progenitor distributions is similar. For sources with count rate $< 1 \text{ cts s}^{-1}$ the new initial spatial distribution results in larger number of young sources. These are objects behind the Gould Belt in OB associations. Outside the Gould Belt the new distribution is more compact than the old one: most of associations are closer than 2 kpc (in the old model NSs were uniformly distributed in the disc up to 3 kpc).

As the next step we compare the results for the old simple ISM model (white bars in Fig. 8 and Fig. 9) with those obtained using the new analytical model (black bars). In both cases we use the new initial progenitor distribution. In general, calculations with the old ISM model produce more observable sources (which can also be seen in the $\log N -$

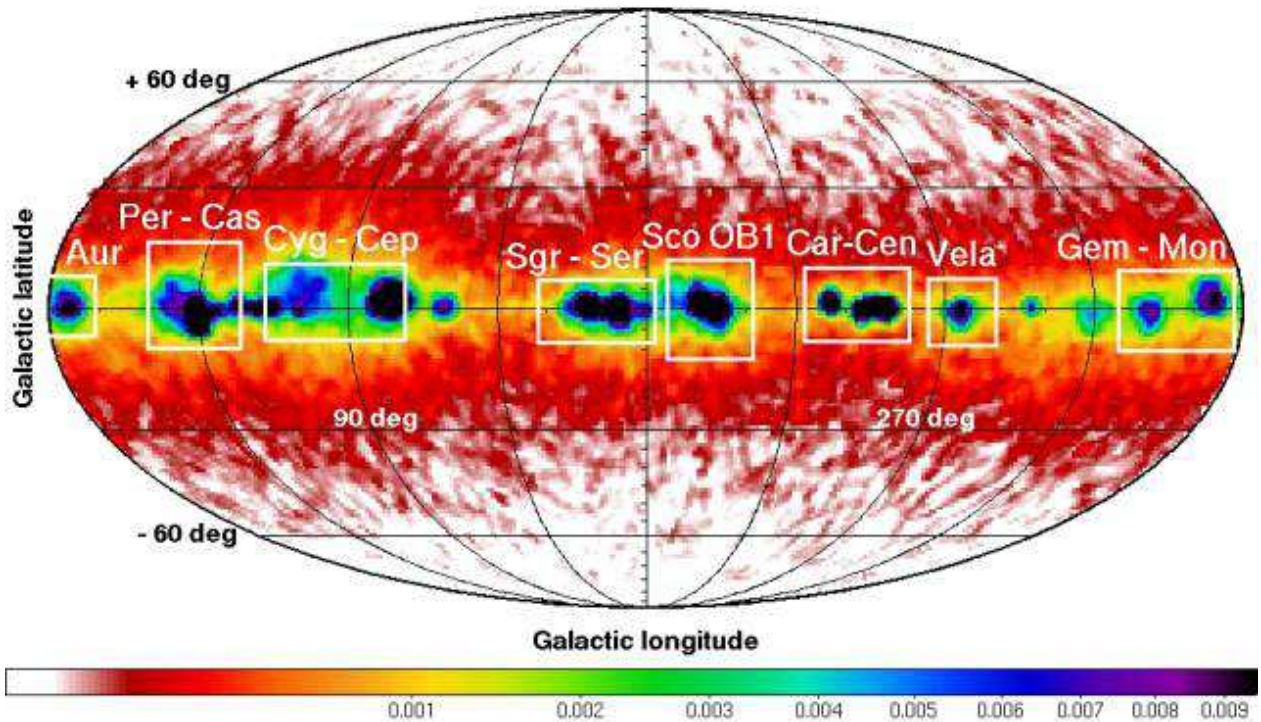


Fig. 7. Same as Fig. 6, but here only faint sources with ROSAT PSPC count rates between 0.001 cts s^{-1} and 0.01 cts s^{-1} are considered. Marked are regions of the corresponding OB associations giving birth to the neutron stars. These OB associations have distances between 1 kpc and 2 kpc. **For an updated version of this figure see Fig. A.3 in the Appendix A.**

log S curves in Fig. 5). **The following detailed comparison of the analytical and Hakkila ISM model for specific directions is obsolete after correcting for the bug in our population synthesis code and can be neglected. The general picture however remains unchanged.** This difference is more clearly pronounced for faint sources with count rates below 1 cts s^{-1} and ages below 3×10^5 years. The X-ray emission of these objects must be more absorbed in the new analytical ISM model to explain this effect. Therefore, these young faint sources have to be located on directions which correspond to larger hydrogen column densities in the new analytical ISM model. Indeed, there are several small regions of higher column density in the Galactic plane, and some of them hinder the view to star associations, e.g. at $l = 215^\circ$.

The distance histograms at different count rates at low distances (e.g. up to the third distance bin, [280, 420] pc) show no difference or only slight reduction comparing the resulting numbers from applying the old ISM with those obtained by using the new analytical ISM model. At larger distances in the distance histograms there are fewer observable NSs in the case of the new analytical model in comparison with the old one, e.g. in the last distance bin, [560, 700] pc, in case of the faintest sources. These differences are evident from the properties of the new analytical ISM model. First, due to the inhomogeneities in the new analytical ISM model there are regions of higher column density compared to the old model. Second, the “average” column density (without apparent ISM clumps) in the Galactic plane is less for the new model at distances below 450 pc.

The lower average $N(\text{H})$ value at relatively close distances can explain the comparable or even slightly increased

predicted number of observable neutron stars even with present ISM clumps. The ISM clumps are however responsible for the number reduction in the right part of the distance histograms. For example there is strong absorption towards the direction $l = 100^\circ$, $b = -5^\circ$ relatively close to the Cygnus-Cepheus OB-associations region. The predicted number of observable NSs is reduced there. Since the OB associations towards this direction of sight are at distances larger than 500 pc (e.g. Cyg OB7 at 740 pc, Cep OB2 at 700 pc and Cep OB3 at 900 pc, Cam OB1 at 900 pc) the effect is pronounced mostly at faint count rates (objects relatively far away).

Now we compare the predicted numbers calculated using the analytical ISM model (black bars) and the Hakkila extinction model (diagonal stripes). Here, we note again that up to a distance of 230 pc both ISM models are almost the same. From 240 pc the extinction study by Hakkila et al. (1997) is applied, and so starting from this point the absorption in this more inhomogeneous model is usually much larger than in the case of the analytical model which is characterized by slower and more homogeneous increase of the column density. Only at distances around 450 pc do the hydrogen column densities of the analytical ISM model become larger than those of the Hakkila ISM model in most regions. For example, the Hakkila ISM model has in general lower hydrogen column densities at $|b| > 10^\circ$ for distances larger than 400 pc. Extinction is also low in this ISM model from $l = 230^\circ$ to $l = 285^\circ$ in the Galactic plane (all distances), where differences of up to an order of magnitude can be reached in comparison to the analytical ISM model.

In agreement with the log N–log S curves of Fig. 5 the

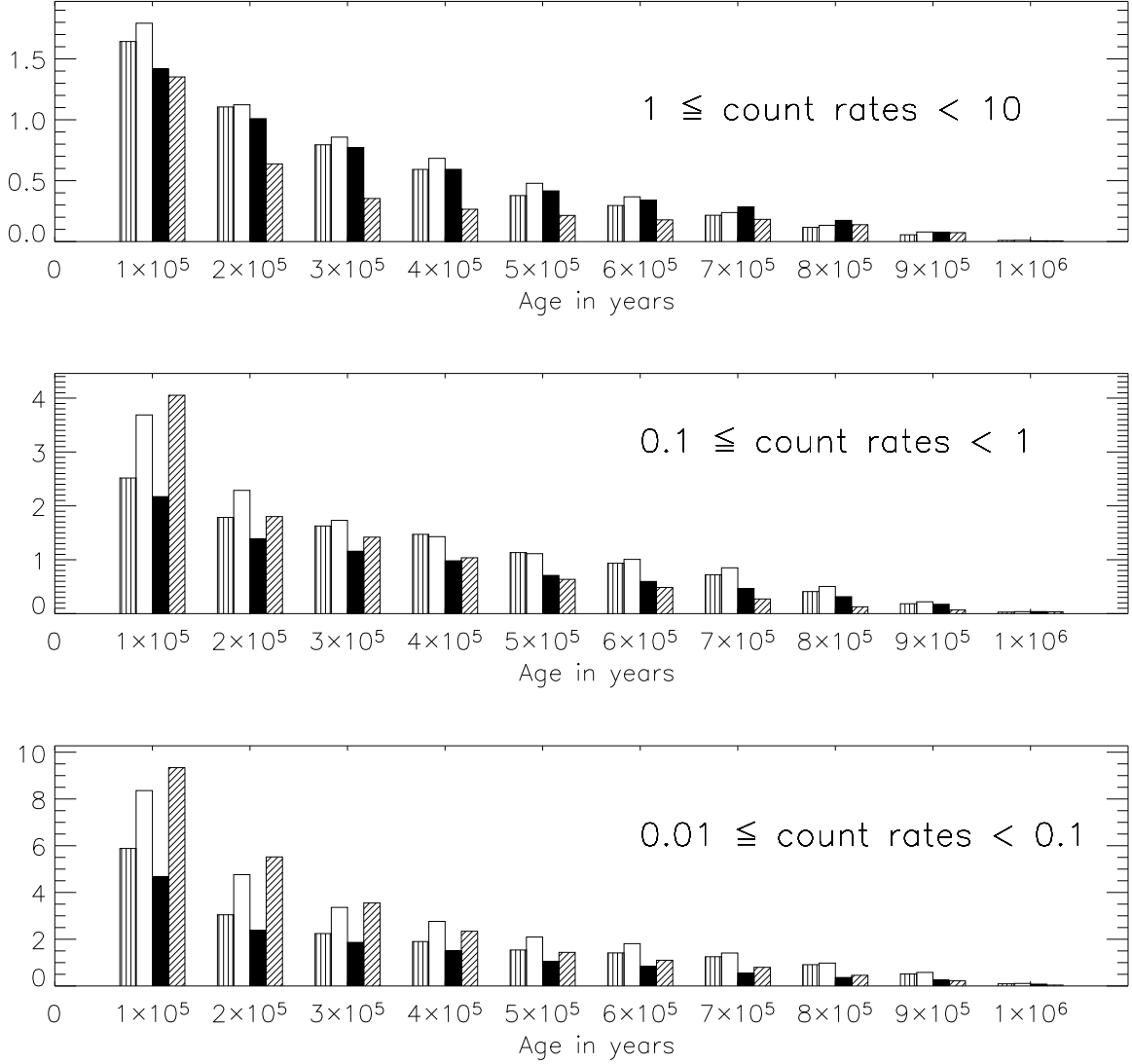


Fig. 8. In this figure the age histograms of observable INSs with thermal X-ray emission are plotted. Three different ROSAT count rate intervals represent very bright, bright and moderately bright ROSAT X-ray sources (note the RASS Bright Source Catalogue limiting count rate of 0.05 cts s^{-1} ; Voges et al. 1999). Different bars correspond to different variants of our model. The bars with vertical stripes indicate the results of the old population synthesis model with a Gould Belt radius of 500 pc (Paper II, see also Sec. 3.1), the white bar corresponds to the population synthesis applying the new initial spatial distribution (Sec. 3.1, reference $\log N - \log S$ curve in Fig. 3 to Fig. 5). Results obtained in the frame of the new analytical ISM model are shown with black bars, and those obtained with the Hakkila ISM model are represented by bars with diagonal stripes (see Sec. 3.2 and Fig. 5 for the corresponding $\log N - \log S$ curves). Please note different y-scales in different panels. **For an updated version of this figure see Fig. A.4 in the Appendix A.**

Hakkila NS number of bright sources is slightly less than in the case of the analytical model, both in the age and the distance histograms. This slightly lower observable NS number is due to larger absorption at closer distances. For count rates below 1 cts s^{-1} the application of the Hakkila ISM leads to a higher number of observable NSs, especially of young age. The lower absorption at large distances explains these higher observable number of ICoNSs. For the discussed distance range, however, the distance histograms indicate only small differences for sources fainter than 1 cts s^{-1} .

4.4. Resultant search strategies

The main aim of this study is to make advances in the strategy for searching for new ICoNSs. Based on the results presented above we can suggest some modifications in the approach to look for new candidates. According to what we discussed in the previous sections, new candidates expected to be identified at ROSAT count rates $< 0.1 \text{ cts s}^{-1}$ should be young objects born in rich OB associations behind the Gould Belt. Most of the recent studies Agüeros et al. (2006); Chierigato et al. (2005); Rutledge et al. (2003) looked for new candidates far from the Galactic plane. It seems that this is not very promising. Our results indicate that ICoNS should be searched in

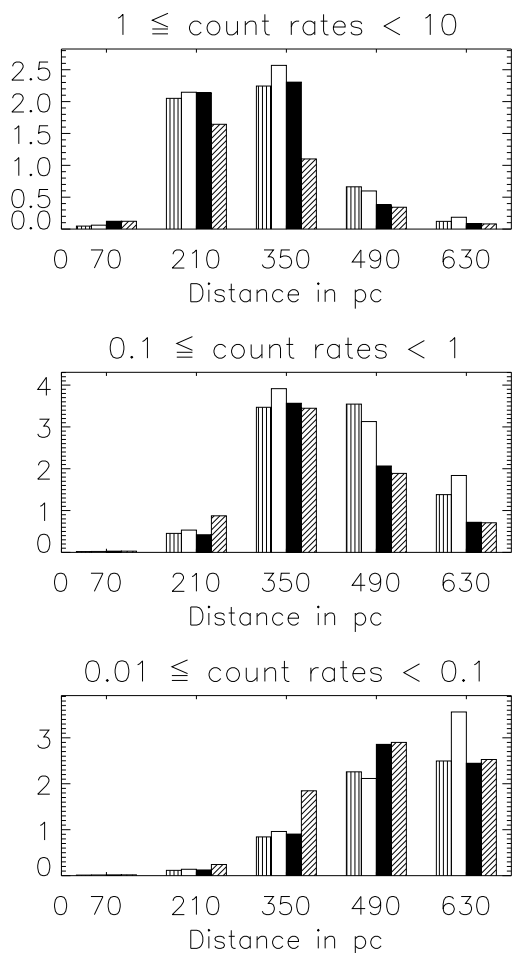


Fig. 9. The distance histograms of the observable ICoNSs with thermal X-ray emission are shown for three different ROSAT count rate intervals. Different bars correspond to different variants of our model, and have the same pattern as in Fig. 8. Please note different y-scales in different panels. **For an updated version of this figure see Fig. A.5 in the Appendix A.**

directions of OB associations such as Cyg OB7 and Cep OB3. On average, new candidates should be slightly hotter than the known ICoNSs, as they are younger.

The absence of sources in the second Galactic quadrant (Motch et al. 2007) can be naturally explained taking into account the properties of close-by OB associations. Most of the associations (Per OB2, Cas-Tau, α Per, Cep OB6) marked in this empty region in Fig. 3 from Motch et al. (2007) have ages which do not favor the appearance of young observable NSs at present times. They are too young (< 7 Myrs) or too old (> 25 Myrs), see Table 1 above. As noted above, the strong contribution of the Cygnus-Cepheus region to the expected neutron star number, shown in map Fig. 6, comes especially at low count rates. Thus, we expect that sources with $50^\circ < l < 200^\circ$ would be identified having lower fluxes than the known sources, since they come from OB associations further away.

Considering sky coverage the ROSAT All Sky Survey (RASS) is currently the best choice to look for new ICoNSs in the Cygnus-Cepheus region which is, according to our presented results, the most promising region. However, the

relatively large positional error circle of ROSAT usually includes many possible optical counterparts, especially at these low Galactic latitudes. Furthermore one has to exclude variable X-ray sources to find ICoNSs. In this respect the recently published XMM-Newton Slew Survey (EPIC with *medium* filter, e.g. Esquej et al. 2006) may become an important database. Currently this survey (0.2–12 keV band) covers roughly 15 % of the sky, and below 2 keV its sensitivity is comparable to that of the RASS (Freyberg et al. 2006). The sensitivity is however strongly inhomogeneous perpendicular to the slew direction. The astrometric accuracy is around $17''$ (90% confidence level), but in few cases an error of $1'$ due to an attitude problem has been reported¹. In conjunction with the RASS, the XMM-Newton Slew Survey with its increasing coverage can be used to identify non-variable X-ray sources and eventually improve their positional accuracy. With the planned expanded energy range down to 150 eV (M.Freyberg, pers. comm.) the soft X-rays emitted by ICoNSs could be detected. However, the XMM-Newton Slew Survey has strongly inhomogeneous sensitivity, and the RASS is not deep enough for the expected new faint sources. Positions of both can be too inaccurate in the highly populated Galactic plane. Pointed observations by XMM-Newton with its high sensitivity and by *Chandra* with its superb positional accuracy may solve these problems for particular directions.

4.5. Outlook

Whether the calculated log N–log S curves are realistic descriptions of the ICoNS numbers also at low count rates could be best tested with the help of an All Sky Survey like that with the planned eROSITA². This experiment is expected to have an angular resolution of $< 25''$ and to be 30 times more sensitive than the RASS (Predehl et al. 2006). eROSITA’s CCD technology is based on an improved concept of the successful XMM-Newton EPIC-pn CCDs. While the noise at low X-ray energies is expected to be much lower compared to the EPIC-pn CCDs (Meidinger et al. 2006) the influence of the planned eROSITA filter actually reduces the sensitivity to or below that of ROSAT in case of energies lower than 0.2 keV (P. Predehl, pers. comm.). Using a preliminary eROSITA response matrix one can estimate that detections of soft blackbody spectra are possible with approximately one eighth of the RASS count rate after the planned 4 years of survey observations. Thus, in principle, sources could be expected to reach count rates down to $\log S \approx -2.7$ (using $0.017 \text{ counts s}^{-1}$ as the RASS limit). This can result in a significant increase in the number of currently known ICoNSs, up to an order of magnitude. However, the actual number of identified NSs will depend strongly on the finally reached positional accuracy, especially in the Galactic plane. For finding new sources of the Magnificent Seven type it will be advantageous to have X-ray positions with $\sim 1''$ accuracy to avoid confusion with faint extragalactic objects (Trümper 2006).

Besides the standard approach based on X-ray/optical wavelengths we mention below other possibilities to look for ICoNSs. They are not directly related to our PS results.

¹ http://xmm.esac.esa.int/external/xmm_science/slew_survey/xmmsl

² www.mpe.mpg.de/erosita/MDD-6.pdf

Keeping the restrictions of our model in mind, however, they may be important in terms of finding new ICoNSs.

Recently, Crawford et al. (2006) found 56 well-determined EGRET error boxes devoided of radio pulsars. Estimates of the number of young NSs which can manifest themselves as γ -ray sources show that many of the 56 sources can be related to these compact objects, but a significant fraction of them should not appear as standard radio pulsars (Harding et al. 2007; Gonthier et al. 2007). Depending on the γ -ray emission model the fraction of Geminga-like objects can reach between 30 % and 90 % of γ -ray pulsars according to Harding et al. (2007). They can be detectable in soft X-rays as *coolers*, elusive in the radio band³. New GLAST and AGILE observations can provide much smaller error boxes, so soon it could be possible to identify sources if they are ICoNSs. It would be fascinating to find more “ γ -ray selected” *coolers*. Of course, it is important to make a joint population synthesis for thermal and non-thermal X-ray sources, but this task is out of the scope of this paper.

Another possibility to find new ICoNSs is to search for (un)bound compact companions of OB runaway stars. More than one hundred OB runaway stars are known in a 1 kpc region around the Sun (de Zeeuw et al. 1999). In comparison with typical OB stars they are characterized by large spatial velocities or/and by large distances from the Galactic plane. Two main origins of these large velocities are currently discussed: dynamical interaction and expulsion of a companion in a close binary system (e.g. Blaauw 1961). The latter case is interesting for the discussion of search for new close-by cooling NSs.

A binary can survive after the first SN explosion in, roughly, 10-20 % of cases (e.g. Popov & Prokhorov 2006). Then a runaway system consisting of an OB star and a compact object (most probably a NS) is expected. A young NS can appear as a radio pulsar. Sayer et al. (1996) and Philp et al. (1996) searched for radio pulsar companions of ~ 40 runaway OB stars. Nothing was found. This result is consistent with the assumption that in less than 20% cases OB stars have radio pulsar companions. Still, it is interesting to speculate that runaway massive stars can have ICoNS as companions. Then a companion can be identified as a source of additional X-ray emission if a NS is younger than $\sim 10^6$ yrs. It is expected to have a thermal component with $T \sim 50 - 200$ eV and $L \sim 10^{30} - 10^{32}$ erg s⁻¹ in most standard scenarios of cooling (see Blaschke et al. (2004); Page & Reddy (2006); Page et al. (2007) and references therein). Our simple estimates show that a cooling NS in a binary with an OB star can appear in the propeller stage. In this case additional energy output non-related to the surface thermal emission can be expected.

As mentioned above, in our calculations very few NSs can reach high Galactic latitudes. However, in our model we do not take into account that progenitors themselves can be high velocity objects (runaway stars or so-called hyper-velocity stars, Brown et al. 2005). In this case a NS can be born far away from the Galactic plane. This possibil-

ity is important in connection with the recently discovered source, Calvera (Rutledge et al. 2007), which could have had a high velocity progenitor. Recent strict bounds on the radio emission from Calvera (Hessels et al. 2007) make it probable that this source is similar to the *Magnificent Seven*.

Hyper-velocity stars (Brown et al. 2007) are expected to originate mainly from the Galactic center. They acquire large velocities after binary disruption in the field of the supermassive Galactic black hole. Another possibility is the ejection from young star clusters (Gvaramadze et al. 2007). Initial velocities are about 1000 – 3000 km s⁻¹. In 25 Myr (maximum lifetime of a NS progenitor) a hyper-velocity star can travel up to 50 kpc, more than enough to explain Calvera. However, the number of such stars is not high. The total rate of production of hyper-velocity stars of all masses is between 10⁻³ and 10⁻⁶ yr⁻¹ (Brown et al. 2007). If we take this rate as $\sim 10^{-6}$ yr⁻¹ for NS progenitors then one can expect a few ICoNS on very high Galactic latitudes. In this case it is not very probable to find one Calvera in ~ 10 kpc from us. Still, this possibility cannot be excluded. The high velocity tail of runaway stars corresponds to 200-300 km s⁻¹. In 25 Myr a NS progenitor can reach $z \sim 5$ kpc above the Galactic plane. Potentially, it is enough to explain Calvera, but detailed modelling is desirable.

Of course population synthesis models in general, and the one we use in particular, cannot predict new types of sources, since our results do not include populations of coolers absolutely different from those assumed in the model. For example, Calvera can be an evolved version of the Cas A central compact object (CCO, for more information on CCOs see e.g. Kaspi et al. 2006). Our model does currently not include objects like this (small emitting area, etc.). In general, the differences in properties between CCOs and close-by coolers indicate that we currently do not understand initial properties (and perhaps, evolution) of NSs well enough.

A joint population synthesis of all known types of NSs would be useful. The presented population synthesis model cannot take into account all interesting possibilities related to evolution of cooling NSs. So, as usual, surprises are not excluded.

5. Conclusions

In this paper we presented our new more advanced model for population synthesis of close-by cooling NSs. The two, slightly different, mass distributions we consider result in nearly the same observable number of NSs. Detailed treatment of the initial spatial distribution of NS progenitors and a detailed ISM structure up to 3 kpc allow us to discuss the strategy to look for new ICoNS. Our main results in this respect are the following: new candidates are expected to be identified behind the Gould Belt, in directions to rich OB associations, in particular in the Cygnus-Cepheus region; new candidates, on average, are expected to be hotter than the known population of ICoNS. Besides the usual approach (looking for soft X-ray sources), the search in ‘empty’ γ -ray error boxes or among run-away OB stars may yield new X-ray thermally emitting NS candidates.

Acknowledgements. We thank D. Blaschke, H. Grigorian, and D. Voskresensky for data on cooling curves and discussions; A. Mel’nik for discussion of properties of OB associations; R. Lallement for the sodium data; and A. Pires for discussions about the ISM model.

³ Geminga itself was claimed to be detected in radio Malofeev & Malov (1997), but the “second Geminga” – 3EG J1835+5918 – is observed only in γ and in soft X-rays.

The authors thank the anonymous referee for careful reading of the manuscript and the suggested improvements.

S.B.P. was supported by INTAS and Dynasty foundations.

This research has made use of SAOImage DS9, developed by Smithsonian Astrophysical Observatory; the SIMBAD and VizieR databases, operated at CDS, Strasbourg, France; and NASA's Astrophysics Data System Bibliographic Services.

References

- Agüeros, M. A., Anderson, S. F., Margon, B., et al. 2006, *AJ*, 131, 1740
- Aguilera, D. N., Pons, J. A., & Miralles, J. A. 2007a, *ArXiv e-prints*, 710
- Aguilera, D. N., Pons, J. A., & Miralles, J. A. 2007b, *ArXiv e-prints*, 712
- Arzoumanian, Z., Chernoff, D. F., & Cordes, J. M. 2002, *ApJ*, 568, 289
- Becker, W., Kramer, M., Jessner, A., et al. 2006, *ApJ*, 645, 1421
- Blaauw, A. 1961, *Bull. Astron. Inst. Netherlands*, 15, 265
- Blaes, O. & Madau, P. 1993, *ApJ*, 403, 690
- Blaha, C. & Humphreys, R. M. 1989, *AJ*, 98, 1598
- Blaschke, D., Grigorian, H., & Voskresensky, D. N. 2004, *A&A*, 424, 979
- Brown, W. R., Geller, M. J., Kenyon, S. J., & Kurtz, M. J. 2005, *ApJ*, 622, L33
- Brown, W. R., Geller, M. J., Kenyon, S. J., Kurtz, M. J., & Bromley, B. C. 2007, *ApJ*, 660, 311
- Chierigato, M., Campana, S., Treves, A., et al. 2005, *A&A*, 444, 69
- Crawford, F., Roberts, M. S. E., Hessels, J. W. T., et al. 2006, *ApJ*, 652, 1499
- Dambis, A. K., Mel'nik, A. M., & Rastorguev, A. S. 2001, *Astronomy Letters*, 27, 58
- de Zeeuw, P. T., Hoogerwerf, R., de Bruijne, J. H. J., Brown, A. G. A., & Blaauw, A. 1999, *AJ*, 117, 354
- Dickey, J. M. & Lockman, F. J. 1990, *ARA&A*, 28, 215
- Esquej, M. P., Altieri, B., Bermejo, D., et al. 2006, in *ESA SP-604: The X-ray Universe 2005*, ed. A. Wilson, 965
- Faucher-Giguère, C.-A. & Kaspi, V. M. 2006, *ApJ*, 643, 332
- Freyberg, M. J., Altieri, B., Bermejo, D., et al. 2006, in *ESA SP-604: The X-ray Universe 2005*, ed. A. Wilson, 913
- Fritze-v. Alvensleben, U. 2000, in *ASP Conf. Ser. 221: Stars, Gas and Dust in Galaxies: Exploring the Links*, ed. D. Alloin, K. Olsen, & G. Galaz, 179
- Fux, R. & Martinet, L. 1994, *A&A*, 287, L21
- Gonthier, P. L., Story, S. A., Clow, B. D., & Harding, A. K. 2007, *Ap&SS*, 309, 245
- Grenier, I. A. 2000, *A&A*, 364, L93
- Grenier, I. A. 2004, *ArXiv Astrophysics e-prints*
- Gvaramadze, V. V., Gualandris, A., & Portegies Zwart, S. 2007, *ArXiv Astrophysics e-prints*
- Haberl, F. 2007, *Ap&SS*, 308, 181
- Haberl, F., Turolla, R., de Vries, C. P., et al. 2006, *A&A*, 451, L17
- Hakkila, J., Myers, J. M., Stidham, B. J., & Hartmann, D. H. 1997, *AJ*, 114, 2043
- Harding, A. K., Grenier, I. A., & Gonthier, P. L. 2007, *Ap&SS*, 309, 221
- Heger, A., Fryer, C. L., Woosley, S. E., Langer, N., & Hartmann, D. H. 2003, *ApJ*, 591, 288
- Heger, A., Woosley, S. E., & Spruit, H. C. 2005, *ApJ*, 626, 350
- Hessels, J. W. T., Stappers, B. W., Rutledge, R. E., Fox, D. B., & Shevchuk, A. H. 2007, *ArXiv e-prints*, 710
- Hobbs, G., Lorimer, D. R., Lyne, A. G., & Kramer, M. 2005, *MNRAS*, 360, 974
- Kaspi, V. M., Roberts, M. S. E., & Harding, A. K. 2006, *Isolated neutron stars (Compact stellar X-ray sources)*, 279
- Keane, E. F. & Kramer, M. 2008, *MNRAS*, 391, 2009
- Kent, S. M., Dame, T. M., & Fazio, G. 1991, *ApJ*, 378, 131
- Kharchenko, N. V., Piskunov, A. E., Röser, S., Schilbach, E., & Scholz, R.-D. 2005a, *A&A*, 440, 403
- Kharchenko, N. V., Piskunov, A. E., Röser, S., Schilbach, E., & Scholz, R.-D. 2005b, *A&A*, 438, 1163
- Lallement, R., Welsh, B. Y., Vergely, J. L., Crifo, F., & Sfeir, D. 2003, *A&A*, 411, 447
- Malofeev, V. M. & Malov, O. I. 1997, *Nature*, 389, 697
- Meidinger, N., Andritschke, R., Hälker, O., et al. 2006, in *High Energy, Optical, and Infrared Detectors for Astronomy II*. Edited by Dorn, David A.; Holland, Andrew D.. *Proceedings of the SPIE*, Volume 6276, pp. (2006).
- Mel'nik, A. M. & Efremov, Y. N. 1995, *Astronomy Letters*, 21, 10
- Miyamoto, M. & Nagai, R. 1975, *PASJ*, 27, 533
- Motch, C., Pires, A. M., Haberl, F., & Schwope, A. 2007, *Ap&SS*, 308, 217
- Ofek, E. O. 2009, *PASP*, 121, 814
- Page, D., Geppert, U., & Küker, M. 2007, *Ap&SS*, 308, 403
- Page, D. & Reddy, S. 2006, *Annual Review of Nuclear and Particle Science*, 56, 327
- Perryman, M. A. C. & ESA. 1997, *The HIPPARCOS and TYCHO catalogues. Astrometric and photometric star catalogues derived from the ESA HIPPARCOS Space Astrometry Mission (The Hipparcos and Tycho catalogues. Astrometric and photometric star catalogues derived from the ESA Hipparcos Space Astrometry Mission, Publisher: Noordwijk, Netherlands: ESA Publications Division, 1997, Series: ESA SP Series vol no: 1200, ISBN: 9290923997)*
- Philp, C. J., Evans, C. R., Leonard, P. J. T., & Frail, D. A. 1996, *AJ*, 111, 1220
- Pichardo, B., Martos, M., & Moreno, E. 2004, *ApJ*, 609, 144
- Piskunov, A. E., Kharchenko, N. V., Röser, S., Schilbach, E., & Scholz, R.-D. 2006, *A&A*, 445, 545
- Popov, S., Grigorian, H., Turolla, R., & Blaschke, D. 2006, (**Paper III**) *A&A*, 448, 327
- Popov, S. B., Colpi, M., Prokhorov, M. E., Treves, A., & Turolla, R. 2000, *ApJ*, 544, L53
- Popov, S. B., Colpi, M., Prokhorov, M. E., Treves, A., & Turolla, R. 2003, (**Paper I**) *A&A*, 406, 111
- Popov, S. B. & Prokhorov, M. E. 2004, *ArXiv Astrophysics e-prints astro-ph/0411792*
- Popov, S. B. & Prokhorov, M. E. 2006, *MNRAS*, 367, 732
- Popov, S. B., Turolla, R., Prokhorov, M. E., Colpi, M., & Treves, A. 2005, (**Paper II**) *Ap&SS*, 299, 117
- Popov, S. B., Pons, J. A., Miralles, J. A., Boldin, P. A., & Posselt, B. 2010, *MNRAS*, 401, 2675
- Pöppel, W. 1997, *Fundamentals of Cosmic Physics*, 18, 1
- Posselt, B., Popov, S. B., Haberl, F., et al. 2007, *Ap&SS*, 308, 171
- Predehl, P., Hasinger, G., Böhringer, H., et al. 2006, in *Space Telescopes and Instrumentation II: Ultraviolet to Gamma Ray*. Edited by Turner, Martin J. L.; Hasinger, Günther. *Proceedings of the SPIE*, Volume 6266.
- Rutledge, R. E., Fox, D. B., & Shevchuk, A. H. 2007, *ArXiv e-prints astro-ph/0705.1011*, 705
- Rutledge, R. E., Fox, D. W., Bogosavljevic, M., & Mahabal, A. 2003, *ApJ*, 598, 458
- Sayer, R. W., Nice, D. J., & Kaspi, V. M. 1996, *ApJ*, 461, 357
- Schlegel, D. J., Finkbeiner, D. P., & Davis, M. 1998, *ApJ*, 500, 525
- Schwope, A. D., Hambaryan, V., Haberl, F., & Motch, C. 2005, *A&A*, 441, 597
- Takatsuka, T. & Tamagaki, R. 2004, *Progress of Theoretical Physics*, 112, 37
- Tammann, G. A., Loeffler, W., & Schroeder, A. 1994, *ApJS*, 92, 487
- Timmer, F. X., Woosley, S. E., & Weaver, T. A. 1996, *ApJ*, 457, 834
- Torra, J., Fernández, D., & Figueras, F. 2000, *A&A*, 359, 82
- Trümper, J. 2006, in *IAU Symposium, Vol. 232, The Scientific Requirements for Extremely Large Telescopes*, ed. P. Whitelock, M. Dennefeld, & B. Leibundgut, 236–240
- Trümper, J. E., Burwitz, V., Haberl, F., & Zavlin, V. E. 2004, *Nuclear Physics B Proceedings Supplements*, 132, 560
- Voges, W., Aschenbach, B., Boller, T., et al. 1999, *A&A*, 349, 389
- Wilms, J., Allen, A., & McCray, R. 2000, *ApJ*, 542, 914
- Woosley, S. E., Heger, A., & Weaver, T. A. 2002, *Reviews of Modern Physics*, 74, 1015
- Yakovlev, D. G. & Pethick, C. J. 2004, *ARA&A*, 42, 169
- Zane, S. 2007, *Ap&SS*, 308, 259
- Zane, S., Turolla, R., Zampieri, L., Colpi, M., & Treves, A. 1995, *ApJ*, 451, 739
- Zavlin, V. E. 2007, *ArXiv Astrophysics eprints astro-ph/0702426*

Appendix A: Erratum

We report in the following on some details regarding the corrected results obtained by the upgraded version of our population synthesis code. All our main conclusions presented above remain valid.

A.1. Comparison of $\log N - \log S$ distributions for different model modifications

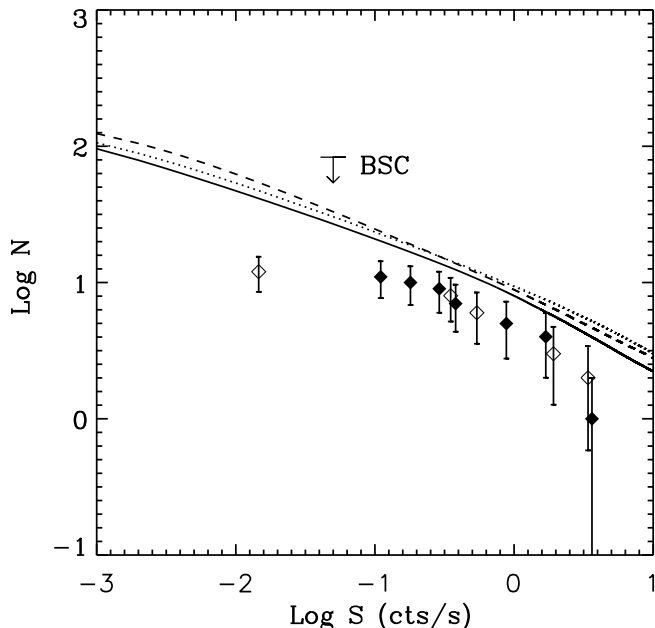


Fig. A.1. $\log N - \log S$ for different X-ray absorbing ISM models. This figure is the corrected version of Fig. 5. All curves are plotted for the new initial spatial distribution, the old mass spectrum and new ISM element abundances. Solid curve: old, simple analytical ISM model as, e.g., in Paper III. Dotted curve: new improved analytical ISM model (corrected); dashed curve: Hakkila ISM model (corrected).

The $\log N - \log S$ curves in Fig. 3 and Fig. 4 of the original paper remain unchanged. The $\log N - \log S$ curves for the new analytical as well as for the Hakkila ISM model in Fig. 5 of the original paper are updated in Fig. A.1. The corrected curves for both ISM models are now situated ≈ 0.3 dex above the observational points. The differences between the Hakkila ISM and the improved ISM analytical model are smaller than those obtained by the original PS-code. However, as before, the application of the Hakkila ISM model results in lower N for high count rates than obtained by using the analytical ISM model, and in higher N for low count rates. Comparison of our new results with observations of bright, cooling NSs indicates that the model overpredicts the number of NSs by roughly a factor of two for both ISM models. The possible reasons for this discrepancy are an inadequate treatment of the NS birth rate or of their thermal evolution, or other, not yet in this paper investigated properties like atmospheres, magnetic fields, or statistical fluctuations. Birth rates of neutron stars are highly uncertain, especially at larger distances (see, e.g., the recent discussions by Keane & Kramer (2008) and Ofek (2009)). However, since probably nearly all the observed XTINSs originate from the Gould Belt we have to discuss the *local* birth rate in the frame of the differences between our PS model predictions and the observational measurements. As discussed in the paper (Sect.

2.1), we adopted a birth rate of 27 Myr^{-1} up to a distance of 500 pc (Grenier 2000; Tammann et al. 1994) and of 270 Myr^{-1} for the whole distance range from 0 to 3000 pc (Tammann et al. 1994). The supernova rate ranges from 17 Myr^{-1} to 27 Myr^{-1} in the entire Gould Belt (Grenier 2004). Only 75% to 87% of the core-collapse supernova produce neutron stars (Heger et al. 2003). Thus, the birth rate in the Gould Belt we chose can be overestimated. However, a factor of two in the *local* birth rate uncertainty seems to be unlikely.

As mentioned in the original paper, the main conclusions about different sets of cooling curves presented in Paper III do not change. The chosen set of cooling curves in this paper actually represents the best choice of the set from Paper III. All other cooling curves from Paper III would result in an even higher $\log N$. It is beyond the scope of this erratum to identify a new cooling curve set that could lead to a $\log N - \log S$ curve in better agreement with observational points.

We further note the possible effect of statistical fluctuations on the uncertainty of the observed $\log N - \log S$ curve, since the overall number of (young enough) neutron stars in the Gould Belt is small. We will evaluate this effect in more detail in a future paper.

A.2. Sky maps

For completeness we show in Figs. A.2 and A.3 the corrected versions of Figs. 6 and 7 from the original paper. The general picture remains the same, but on average more NSs are expected in accordance to the $\log N - \log S$ curve. For bright sources, a subgroup of Sco OB2, Lower Centaurus Crux (de Zeeuw et al. 1999), is predicted to have more observable NSs compared to other Sco OB groups, which was not visible in the map obtained with the original version of the PS code.

A.3. Age and distance distributions

Age and distance diagrams obtained with the corrected PS-code show the same main features as those obtained with the old code except that the NS numbers of the analytical and Hakkila ISM model (the last black and diagonal-striped bars in Figs. 8 and 9 of the original paper) are larger than before, as is expected from the $\log N - \log S$ curves.

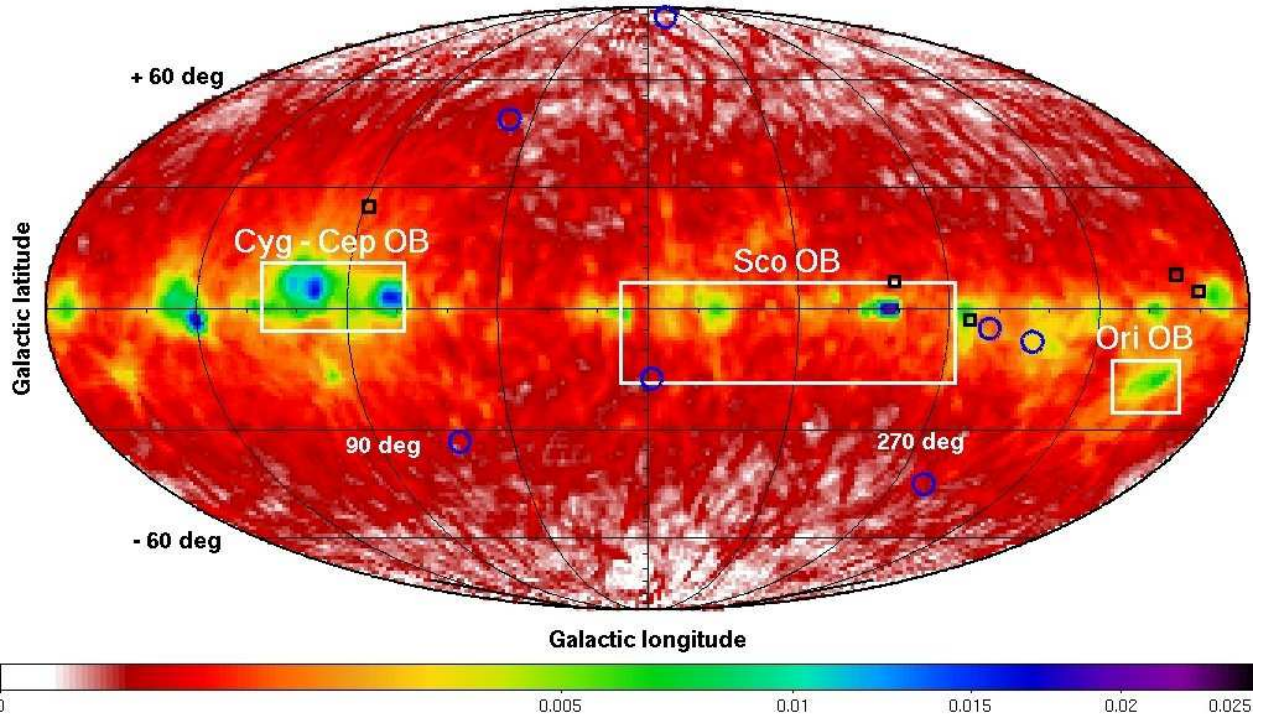


Fig. A.2. This map is the corrected version of Fig.6, showing the expected number density of isolated neutron stars with thermal X-ray emission in units of numbers per square degree. The Galactic map is in Mollweide projection. Only sources with ROSAT PSPC count rates larger than 0.05 cts s^{-1} are considered. Marked in blue are the positions of the Magnificent Seven and in black the positions of close young radio pulsars with detected thermal X-ray emission. Note that the runs for Figs.6 and 7 on the one hand, and Figs. A.2 and A.3 on the other hand, are separate realisations of our code (e.g., randomised birth places); therefore, individual NS "tracks" are not the same.

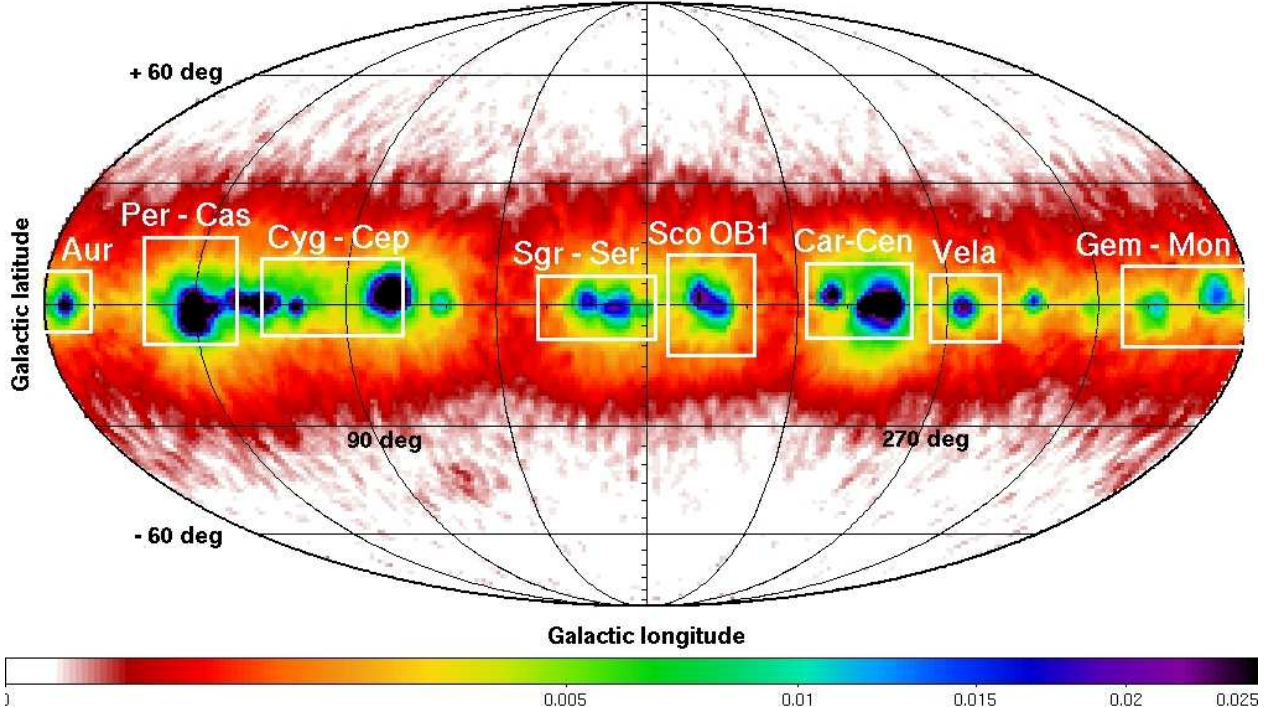


Fig. A.3. This map is the corrected version of Fig.7. Here only faint sources with ROSAT PSPC count rates between 0.001 cts s^{-1} and 0.01 cts s^{-1} are considered.

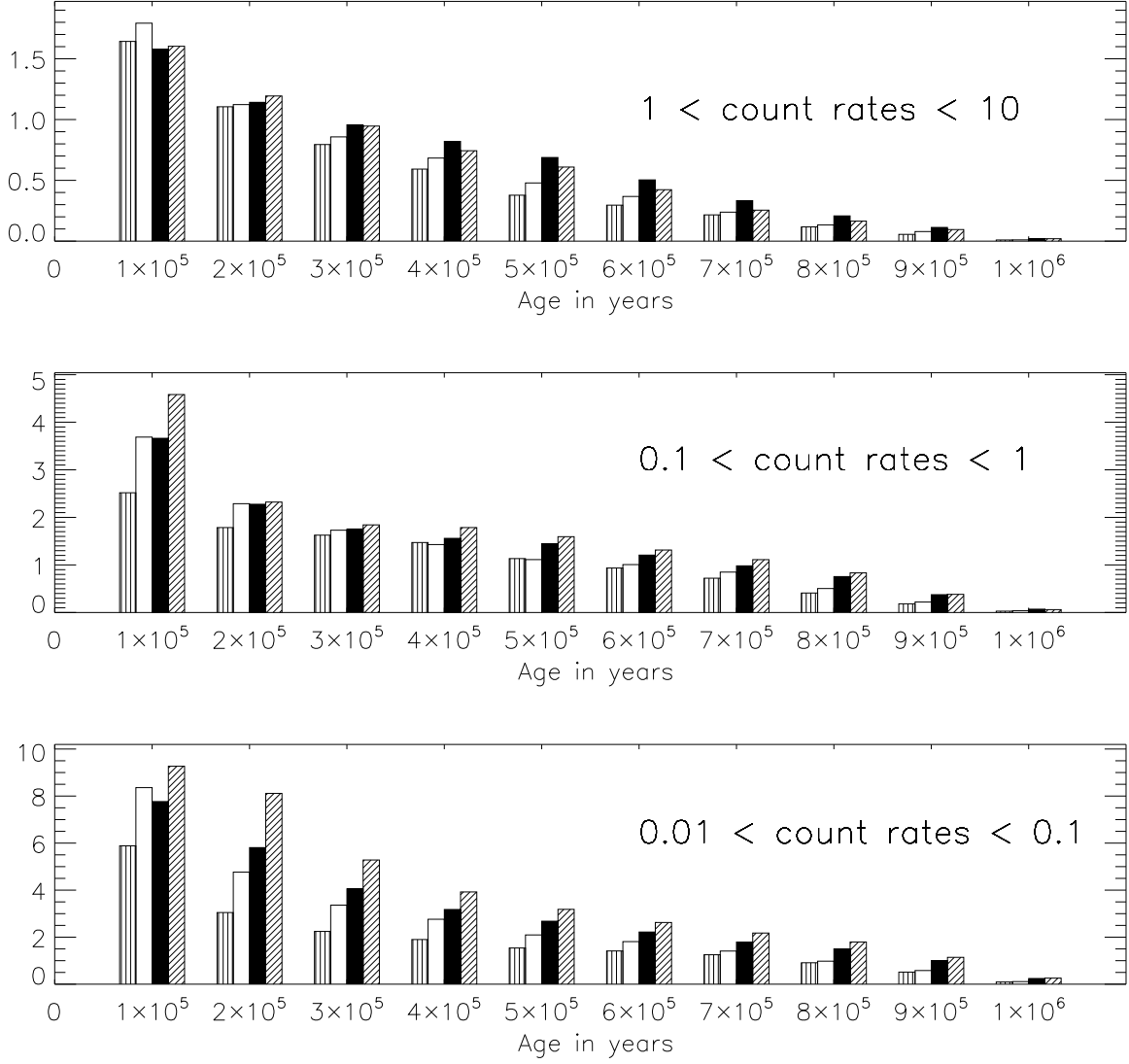


Fig. A.4. This figure is the corrected version of Fig. 8. It shows the age histograms of observable INs with thermal X-ray emission. Three different ROSAT count rate intervals represent very bright, bright and moderately bright ROSAT X-ray sources (note the RASS Bright Source Catalogue limiting count rate of 0.05 cts s^{-1} ; Voges et al. 1999). Different bars correspond to different variants of our model. The same pattern as in Fig. 8 are used: The bars with vertical stripes indicate the results of the old population synthesis model with a Gould Belt radius of 500 pc (Paper II, see also Sec. 3.1), the white bar corresponds to the population synthesis applying the new initial spatial distribution (Sec. 3.1, reference $\log N - \log S$ curve in Fig. 3 to Fig. 5). Results obtained in the frame of the new analytical ISM model (corrected) are shown with black bars, and those obtained with the Hakkila ISM model (corrected) are represented by bars with diagonal stripes (see Sec. 3.2 and Fig. A.1 for the corresponding $\log N - \log S$ curves). Please note different y-scales in different panels.

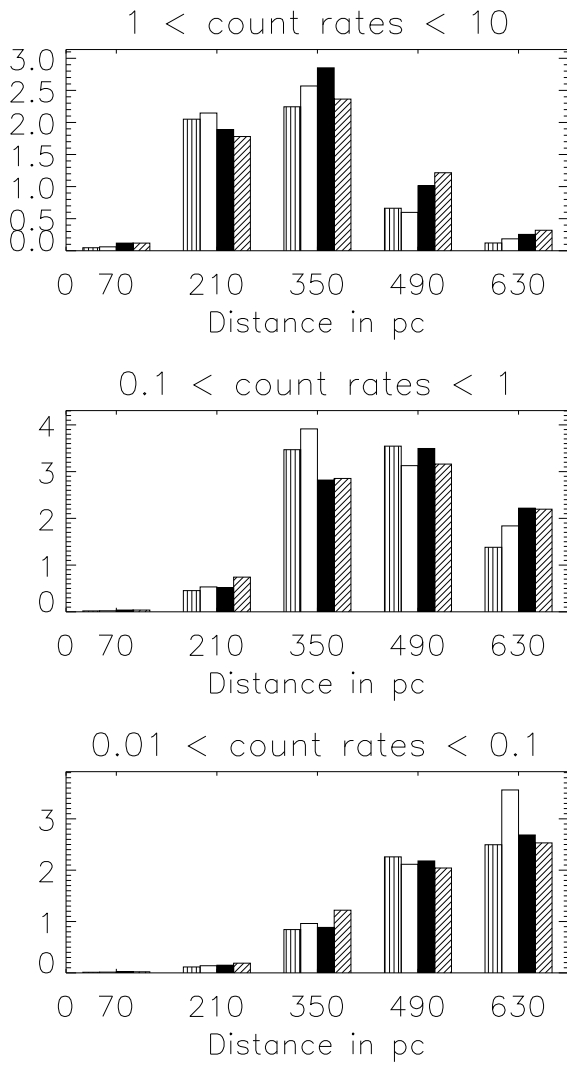


Fig. A.5. This is the corrected version of Fig. 9, the distance histograms of the observable INSs with thermal X-ray emission for three different ROSAT count rate intervals. Different bars correspond to different variants of our model, and have the same pattern as in Fig. 8. Please note different y-scales in different panels.